22nd Australasian Fluid Mechanics Conference AFMC2020
Brisbane, Australia, 7–10 December 2020
https://doi.org/10.14264/d1247d1

Seasonal Variability of Offshore Wind Turbine Wakes

W. Chanprasert[1], R. Sharma[1] J. Cater[2] and S. Norris[1]

[1] Department of Mechanical Engineering
The University of Auckland, Auckland 1010, New Zealand

[2] Department of Engineering Science
The University of Auckland, Auckland 1010, New Zealand

Abstract

The seasonal variations in the stability of the offshore atmospheric boundary layer (ABL) are more significant than diurnal variations because of the high specific heat capacity of water. Atmospheric turbulence is strongly influenced by the atmospheric stability and therefore the variations in wind speed and atmospheric stability are important to wind turbine operations since they affect the power production and fatigue loading. In this study, wind turbine wakes in a wind farm are modelled using Large Eddy Simulation (LES). The air and ocean temperatures and wind speeds measured by a floating buoy are used to prescribe the surface heat flux and wind speed for the simulations. The results show that the wind farm efficiency in winter (unstable ABL) is approximately 20% higher than in summer (stable ABL). The dynamic loads of the upstream turbine were lower in summer due to the weaker ambient turbulence intensity of the stable ABL. The magnitudes of the dynamic loads in winter and summer are comparable, particularly in the high frequency range.

Keywords
LES; Wind Turbines; Wakes

Introduction

There are a number of advantages to siting wind turbines offshore. As well as the large available area and the limited impact on human activity, the lower surface roughness of the sea surface offers a higher mean wind speed and lower turbulence levels [3]. However, the characteristics of the wind can be influenced significantly by the thermal stratification (or stability) of the atmosphere, which can range from a stable, through neutral to an unstable condition [3]. A neutral condition can be observed during strong winds when turbulence generation is dominated by shear due to the surface friction. A stable case can occur when the surface loses heat and causes the air temperature near the surface to be lower than that of the air above. This results in a stable stratification, which suppresses vertical motion and turbulence. An unstable stratification occurs when the surface is heated, warming the adjacent air, thereby promoting vertical motion of the air and increased turbulence.

Wind turbine wakes are affected by the atmospheric stability via atmospheric turbulence [2]. When the ambient turbulence level is relatively high, such as in an unstable ABL, the turbulent mixing in the shear layer of the wakes is enhanced which entrains more free-stream air and results in faster wake recovery. On the other hand, the wake length can be longer when the ambient turbulence is low. Hence, these different atmospheric conditions have a significant impact on the overall wind farm power production and the structural loading of downstream turbines.

For onshore wind farms, the diurnal variations of atmospheric stability and wind speed are significant for the daily power production. However, these short term variations are rarely observed in the offshore environment because of the convective mixing process in the top layers of the ocean which reduces variations in the surface temperature. However, the seasonal variations are more prominent for offshore wind farms; Barthelmie et al. [2] investigated the efficiency of the Nysted offshore wind farm in Denmark and found that the average efficiency in the summer was approximately 10% higher than the winter.

Most LES studies of offshore wind farms have been limited to existing wind farm sites, particularly in Northern Europe such as Horns Rev in Denmark, Lillgrund in Sweden and EnBW Baltic 1 in the Baltic sea [9, 7, 16]. These locations have a meteorological tower that provides a comprehensive ocean and wind data at multiple heights. However, it is of interest to explore the potential of other offshore sites for wind farming, using numerical simulations. In this study, the impact of seasonal variations on wind turbine array performance is determined using LES with an actuator line method where the prescribed wind speed and surface heat flux are obtained from a buoy located off the east coast of the US.

Methodology

MetOcean Data

The offshore meteorological data used in this study was measured by a buoy which is owned and maintained by the National Data Buoy Center [13]. The buoy is located 54 Nautical Miles southeast of Nantucket, Massachusetts at 40.504 N latitude and 69.248 W longitude. Wind speeds and air temperature are measured at approximately 4 m above sea level, while the water temperature is measured 1.5 m below the sea surface.

Figure 1 presents monthly averaged data for wind speed as well as air and sea surface temperatures in 2009. This particular year was chosen because of the data availability. The solid lines are curve fits chosen to highlight the seasonal trends; the fitted values were not used in the simulations. The wind speed is higher in winter than in summer, with differences of approximately 4 m/s at the anemometer-height. The temperature difference varies seasonally, with the water temperature being higher than the air temperature in summer, with the opposite in winter resulting in a reversal of the surface heat fluxes. This is in agreement with [8] which states that an unstable boundary layer is observed in autumn to early winter, and a stable boundary layer in spring to early summer.

In order to model the offshore wind profiles using LES, the surface heat flux, surface roughness and wind speed at turbine hub-height are calculated from the buoy data.

The sensible surface heat flux was calculated from

$$q_s = \rho c_p C_H U (T_s - T_a), \tag{1}$$

where ρ is the air density, c_p is the specific heat capacity of the air, U is the mean wind speed at the reference height, T_s is

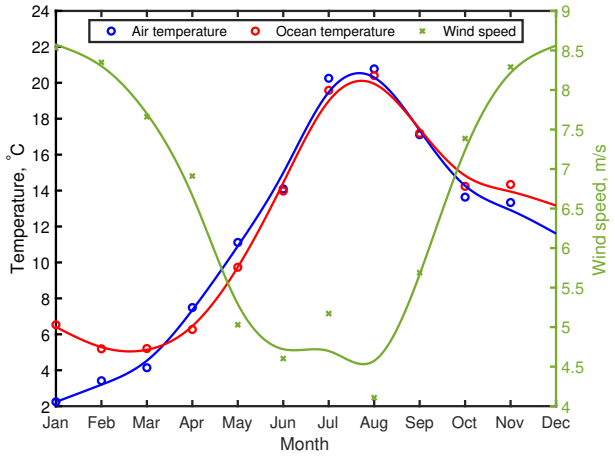

Figure 1. The variations of wind speed, air and ocean temperature at the SE Nantucket site in 2009. The monthly averaged data are represented by the markers 'o' for temperature and '×' for wind speed. Splines are represented by the solid lines to show the predicted trends.

the sea surface temperature, T_a is the air temperature at the reference height, and C_H is the heat flux coefficient. In this study, the heat flux coefficient was derived from published tabular data [14].

The wind speed at hub-height was estimated using the wind profile [8]:

$$u(z) = \frac{u_*}{\kappa}\left[\ln\left(\frac{z}{z_0}\right) + \psi\right], \tag{2}$$

where κ is the von Karman constant, u_* is the friction velocity, z_0 is the surface roughness height, and ψ is the atmospheric stability function, which is typically expressed using the Businger-Dyer relationships [8].

The surface roughness height, z_0, was calculated using Charnock's relation, where the sea surface roughness is calculated as a function of that the friction velocity:

$$z_0 = \frac{\alpha_c {u_*}^2}{g}, \tag{3}$$

in which $g = 9.81 m/s^2$ is the gravitational acceleration and α_c is Charnock's constant. A value of $\alpha_c = 0.0034$ is used in this study which represents a near-coastal area according to the IEC 61400-3 standard [1].

The data for January (winter) and July (summer) are presented in Table 1. The values of the Obukhov length, L, indicate the atmospheric stability, and is classified as unstable in January and stable in July according to [15].

Month	$q_s, W/m^2$	$U_{hub}, m/s$	z_0, m	L, m
January	49.7	11.37	4.9e-4	-89
July	-3.9	7.75	1.3e-4	163

Table 1. The calculated surface heat flux (q_s), wind speed at hub-height (U_{hub}), surface roughness (z_0) and Obukhov length, (L)

SOWFA Code

The Simulator fOr Wind Farm Applications (SOWFA) code is an open-source Computational Fluid Dynamics solver developed at the National Renewable Energy Laboratory (NREL) [4] that calculates atmospheric wind and wind turbine wake flows. The code solves the spatially filtered, incompressible Navier-Stokes equations with the Boussinesq approximation. The equations are discretised using the finite volume method and solved iteratively with the pressure-implicit split-operator (PISO) algorithm. A second-order central differencing scheme is used for spatial discretisation for both the advective and diffusive terms while a second-order implicit scheme is used for time stepping. A Coriolis force was added to the momentum equations, and was calculated for the Earth's angular velocity of 7.27×10^{-5} rad/s and a latitude of 40.5° north matching the buoy's location. The Deardorff-Lilly one-equation subgrid scale (SGS) model was used [12, 10].

The wind turbines were modelled using an actuator line method. The lines which represent the turbine blades were subdivided into discrete elements. The properties of the blade elements including chord length, blade twist angle and lift and drag coefficient were obtained from tabulated aerofoil data. At each time step, the lift and drag forces on the blade elements were calculated from the local relative wind speed and the blade properties. The forces were then distributed to the flow solver mesh using a Gaussian function [4].

Simulation Set-up

There are two steps in the simulation; in the first step, the wind profile and turbulence data were produced by a precursor simulation in which the flow was calculated using a pressure-driven periodic boundary condition for an empty domain. The computational domain size for the Unstable ABL case (January) was $4000\ m \times 3000\ m \times 1000\ m$ in the x, y, z directions with a uniform mesh size of $10\ m$. For the stable ABL case (July), the flow domain was $4000\ m \times 3000\ m \times 500\ m$ while the mesh size was kept the same as the unstable case. The domain for the stable case could be shallower because the height of the stable boundary layer is less than that of the unstable ABL [8]. The mean horizontal wind speed at hub-height was controlled to the U_{hub} specified in Table 1 for each of the simulation cases. The flow direction at hub-height was driven at an angle of 30 degrees to the x-axis. The reason that the flow was not aligned with the x-axis or the y-axis was to avoid a non-uniform mean wind speed developing in the span-wise direction as the flow is periodically cycled across the flow domain [5].

The domain was initialised with the desired hub-height wind speed with small divergence-free perturbation close to the bottom boundary [5]. The initial temperature was set to a constant with a capping inversion temperature profile. The top boundary was set as stress free and adiabatic. The wall shear stress and the temperature flux models were implemented at the bottom boundary. Monin-Obukhov Similarity Theory was used to calculate the friction velocity of the ABL from the prescribed surface roughness height, z_0, and the surface heat flux, q_s given in Table 1 [4]. This surface model allows the use of a uniform mesh without near-wall mesh refinement. The precursor simulations were carried out for 18000 s for the unstable case (winter) and 60000 s for the stable case (summer) which were long enough to obtain a quasi-steady state.

In the second step, the NREL 5-MW reference turbine [11], which has a rotor diameter D, of 126 m and a hub-height H, of 90 m, was modelled. Wind turbine controllers were also modelled in SOWFA, where the five region controller for the generator-torque controller was used for the operating region below the rated wind speed (11.4 m/s) while the blade pitch regulated controller was enabled above the rated point. Four turbines were placed in-line normal to the wind direction as illustrated in Figure 2 with a distance of 7 rotor diameters (7 D) between turbines.

In the first mesh refinement zone around the turbine array (the inner rectangle in Figure 2) the mesh was refined to 2.5 m in all directions in order to better resolve the turbine wakes [5]. A buffer mesh refinement zone (the outer rectangle) of a uniform 5 m cell size was also used. The top and bottom boundary conditions were identical to the precursor simulation. For the inlet boundaries, the velocity and temperature data were specified using the recorded plane data from the precursor simulation. For the outlet boundaries, the velocity and temperature gradients were set to zero.

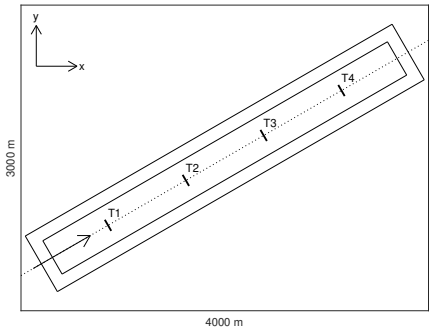

Figure 2. A plan view of the four in-line wind turbines in the flow domain. The two rectangles encompassing the wind turbines indicate the two mesh refinement zones and the arrow denotes the mean inflow direction at hub-height.

Atmospheric Winds

The atmospheric wind profiles were obtained from the precursor simulations. The statistical calculations used the last 2000 s of the simulation time.

Figure 3 shows the mean vertical profiles of the horizontal velocity for January (unstable) and July (stable). The wind shear for the January case, particularly at the rotor height, is lower than the July case. Since the atmospheric stability for July is classified as stable, a low-level jet was predicted at $z/H \approx 3.5$ where the velocity is approximately 20% higher than the velocity near the top boundary [6].

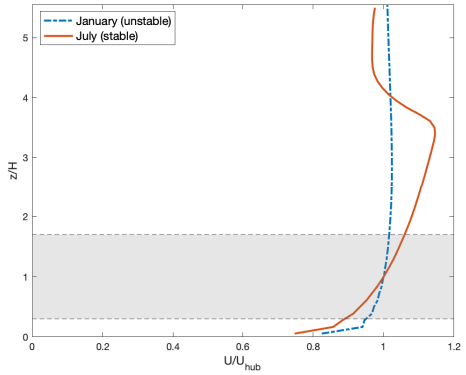

Figure 3. The averaged horizontal velocity profile scaled by the wind speed at hub-height for January (the dash-dot line) and July (the solid line). The gray shaded area represents the turbine rotor height.

The stream-wise turbulence intensity profiles are plotted in Figure 4, where the turbulence intensity at the hub-height for the unstable January case was 9.7% dropping to 5.7% when the ABL stabilised in July.

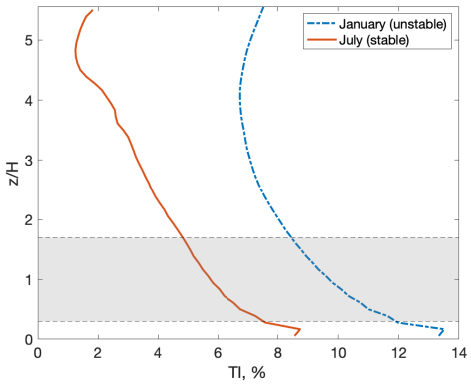

Figure 4. The averaged horizontal turbulence intensity profile of January (the dash-dot line) and July (the solid line). The gray shaded area represents the turbine rotor height.

Wind Farm Simulations

The wind turbine data analysis for both cases was conducted over a sample time of 600 s. Due to the higher wind speed in January, the averaged total power production of the 4-row 5 MW wind turbine array was 14.2 MW which is significantly higher than 3.9 MW in July.

The wind farm efficiency η, was calculated in order to determine the effects of atmospheric stability on the wakes and wind farm performance. It is defined as $\eta = \frac{1}{N_T P_1} \sum_{i=1}^{N_T} P_i$ where N_T is the number of turbines and P_i is the power production of each turbine, with $i = 1$ representing the first row. The efficiency was 77.1% for January and 58.5% for July. The efficiency in July was lower than January as the turbine wakes were longer, and this can be seen in the normalised power output of each turbine row in Figure 5. The power output of all downstream turbines are of similar magnitude. The power losses are approximately 30% in January and increase to more than 50% in July.

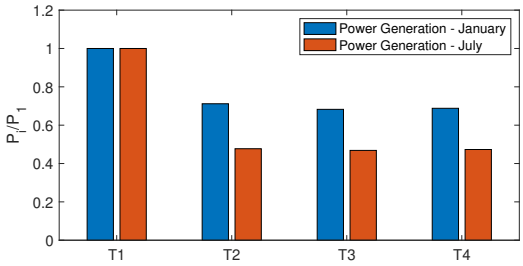

Figure 5. The power generation of each wind turbine normalised by the power output of the first row (P_1).

The wakes also affect the aerodynamic loads on downstream turbines. Figures 6 and 7 present the power spectral density (PSD) plots of the thrust load on the turbines in the first and second rows, respectively. The peaks of the thrust load spectra are each located at "3P" and its harmonics (6P, 9P, ...), where "3P" corresponds to three times the turbine rotational speed, the blade pass frequency.

The first row turbine operates in the free stream flow and it is directly affected by the atmospheric turbulence. The higher turbulence intensity of the unstable ABL in January results in a higher magnitude PSD across the frequency range (Figure 6). For the downstream turbines the loads on the rotor are dominated by the upstream turbine's wake. Although, the overall

patterns for both first and second turbines look similar, the PSD magnitude for the second turbine for the July case in Figure 7 is similar to that for January particularly in the high frequency region. This indicates that the turbulent wakes of the stable ABL in July have more impact on the dynamic loads of the downstream turbines.

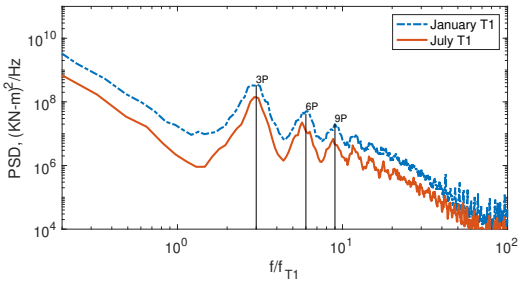

Figure 6. Power spectral density for the thrust load on the first row wind turbine rotor for January and July. The frequency on the x-axis was normalised by the rotational frequency of wind turbines (f_{T1}). The vertical solid lines denote the amplitude peaks at three times the rotational speed and its harmonics.

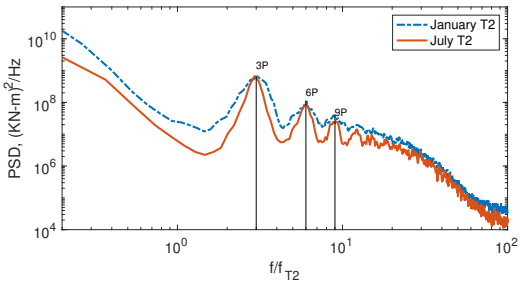

Figure 7. Power spectral density for the thrust load on the second row wind turbine rotor for January and July. The frequency on the x-axis was normalised by the rotational frequency of wind turbines (f_{T2}). The vertical solid lines denote the amplitude peaks at three times the rotational speed and its harmonics.

Conclusions

The seasonal variations of wind speed and atmospheric stability have a significant impact on wind farm power generation, wind farm efficiency and wind turbine dynamic loads. An unstable ABL with a higher mean wind speed in winter results in a higher total power generation and wind farm efficiency. The dynamic loads of the upstream turbine were lower in summer due to a weaker ambient turbulence intensity of the stable ABL. For the downstream turbine located 7D behind the upstream, the magnitude of the dynamic loads for both cases were comparable, particularly at frequencies higher than 10 Hz.

Acknowledgements

The authors would like to acknowledge the NREL National Wind Technology Center for providing the open-source SOWFA solver. The offshore data used in the simulations was obtained from the National Data Buoy Center. The simulations were computed on High Performance Computing facilities provided by New Zealand's eScience Infrastructure (NeSI).

References

[1] Wind turbines-part 3: Design requirements for offshore wind turbines, Standard BS EN IEC 61400-3:2009, International Electrotechnical Commission, 2009.

[2] Barthelmie, R. J. and Jensen, L., Evaluation of wind farm efficiency and wind turbine wakes at the nysted offshore wind farm, *Wind Energy*, **13**, 2010, 573–586.

[3] Burton, T., Jenkins, N., Sharpe, D. and Bossanyi, E., *Wind Energy Handbook (2nd Edition)*, John Wiley & Sons, 2011.

[4] Churchfield, M., Simulator fOr Wind Farm Applications (SOWFA), 2017, National Renewable Energy Laboratory.

[5] Churchfield, M. J., Lee, S., Michalakes, J. and Moriarty, P. J., A numerical study of the effects of atmospheric and wake turbulence on wind turbine dynamics, *Journal of Turbulence*, N14.

[6] Churchfield, M. J., Lee, S. and Moriarty, P. J., Adding complex terrain and stable atmospheric condition capability to the openfoam-based flow solver of the simulator for on/offshore wind farm applications *SOWFA*, in *ITM Web of Conferences, Symposium on OpenFOAM in Wind Energy, 1*, Curran Associates;, Red Hook, 2014, volume 2, 34–49, 34–49.

[7] Dörenkämper, M., Witha, B., Steinfeld, G., Heinemann, D. and Kühn, M., The impact of stable atmospheric boundary layers on wind-turbine wakes within offshore wind farms, *Journal of Wind Engineering and Industrial Aerodynamics*, **144**, 2015, 146–153.

[8] Emeis, S., *Wind energy meteorology, green energy and technology*, Springer, 2013.

[9] Ghaisas, N. S., Archer, C. L., Xie, S., Wu, S. and Maguire, E., Evaluation of layout and atmospheric stability effects in wind farms using large-eddy simulation, *Wind Energy*, **20**, 2017, 1227–1240.

[10] Johlas, H., Martınez-Tossas, L., Lackner, M., Schmidt, D. and Churchfield, M., Large eddy simulations of offshore wind turbine wakes for two floating platform types, in *Journal of Physics: Conference Series*, 2020, volume 1452, 012034, 012034.

[11] Jonkman, J., Butterfield, S., Musial, W. and Scott, G., Definition of a 5-MW reference wind turbine for offshore system development, Technical report, NREL/TP-500-38060, National Renewable Energy Lab. (NREL), Golden, CO (United States), 2009.

[12] Moeng, C.-H., A large-eddy-simulation model for the study of planetary boundary-layer turbulence, *Journal of the Atmospheric Sciences*, **41**, 1984, 2052–2062.

[13] National Oceanic and Atmospheric Administration, National data buoy center, 2019, accessed on 20 June 2019. `https://www.ndbc.noaa.gov/`.

[14] Smith, S. D., Coefficients for sea surface wind stress, heat flux, and wind profiles as a function of wind speed and temperature, *Journal of Geophysical Research: Oceans*, **93**, 1988, 15467–15472.

[15] Wharton, S. and Lundquist, J. K., Assessing atmospheric stability and its impacts on rotor-disk wind characteristics at an onshore wind farm, *Wind Energy*, **15**, 2012, 525–546.

[16] Witha, B., Steinfeld, G., Dörenkämper, M. and Heinemann, D., Large-eddy simulation of multiple wakes in offshore wind farms, *Journal of Physics: Conference Series*, **555**, 2014, 012108.